

LONGSHORTNET: EXPLORING TEMPORAL AND SEMANTIC FEATURES FUSION IN STREAMING PERCEPTION

Chenyang Li^{1*}, Zhi-Qi Cheng^{2*}, Jun-Yan He^{1*}, Pengyu Li¹,
Bin Luo^{1†}, Han-Yuan Chen¹, Yifeng Geng¹, Jin-Peng Lan¹, Xuansong Xie¹

¹DAMO Academy, Alibaba Group

²Carnegie Mellon University

ABSTRACT

Streaming perception is a task of reporting the current state of autonomous driving, which coherently considers the latency and accuracy of autopilot systems. However, the existing streaming perception *only uses the current and adjacent two frames* as input for learning the movement patterns, which cannot model actual complex scenes, resulting in failed detection results. To solve this problem, we propose an end-to-end dual-path network dubbed *LongShortNet*, which captures *long-term temporal motion* and calibrates it with *short-term spatial semantics* for real-time perception. Moreover, we investigate a Long-Short Fusion Module (*LSFM*) to explore spatiotemporal feature fusion, which *is the first work to extend long-term temporal* in streaming perception. We evaluate the proposed LongShortNet and compare it with existing methods on the benchmark dataset Argoverse-HD. The results demonstrate that the proposed LongShortNet *outperforms the other state-of-the-art methods* with almost no extra computational cost¹.

Index Terms— streaming perception, feature fusion

1. INTRODUCTION

Autonomous driving requires the real-time perception of streaming video and reactions to motion changes (e.g., overtaking, turning, etc). Different from the traditional Video Object Detection (VOD) [1, 2, 3, 4, 5, 6, 7, 8, 9, 10, 11, 12, 13, 14], Li et al. proposed a novel autopilot perception tasks, i.e., streaming perception [15]. Streaming perception can realistically simulate autonomous driving scenarios. Typically, it offers a new metric called streaming Average Precision (sAP) to force perception to evaluate accuracy and latency in a consistent manner [15]. *Unlike offline VOD, streaming perception opens up a new direction for online real-time perception for autonomous driving.*

For ease of understanding, Fig. 1 explains the difference between VOD and steaming perception, where the bounding boxes with different colors display the comparison in real scenarios. As stated in the previous work [16], most VOD approaches [17, 18, 19, 20, 21] inevitably yield errors *due*

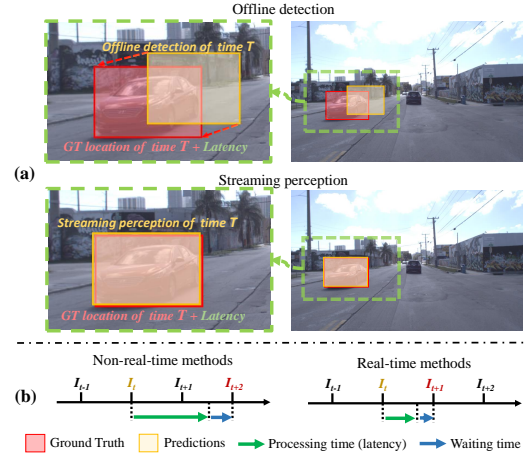


Fig. 1: Offline detection (VOD) vs. streaming perception. (a) shows the comparison in real autonomous driving scenarios. (b) depicts the processing time on the timeline. Unlike Offline detection, streaming perception is *real-time and online*.

to the time delay brought by the offline detection. In contrast, streaming perception either 1) employs trade-offs between speed and accuracy [15, 22] or 2) discards the long-term temporal motions and only uses the last two frames to reduce latency [16]. Although these strategies have made some progress, they cannot handle complex motion and scene shifts *due to the incapacity to account for the short-term spatial and long-term temporal in video streams.*

Going a step further, we reveal severe perceptual issues due to lack of *spatial semantics* and *temporal motion*. Fig. 2 shows the video stream captured by the car’s front-view camera. The state of the detected object in the video stream is affected by its own motion and camera movement. Apart from ideal uniform linear motion, the actual video streams are full of 1) *non-uniform motion* (e.g., vehicle accelerating overtake), 2) *non-straight motion* (e.g., object and camera turning), 3) *scene occlusion* (e.g., billboard and oncoming car occlusion) and 4) *small objects* (e.g., cars and road signs in the distance). Evidently, the motions and scenarios in real autonomous driving are incredibly tricky and uncertain.

Faced with these concerns, StreamYOLO [16] wholly ignores the semantics and motion in video streams, and only uses the last two frames as input (i.e., the current and the previous frames). Because of the absence of spatial semantic and temporal motion cues, it cannot handle complex scenes (such

*C. Li, Z. Cheng, and J. He contribute equally.

†corresponding author

¹The source code is at <https://shorturl.at/BKX78>

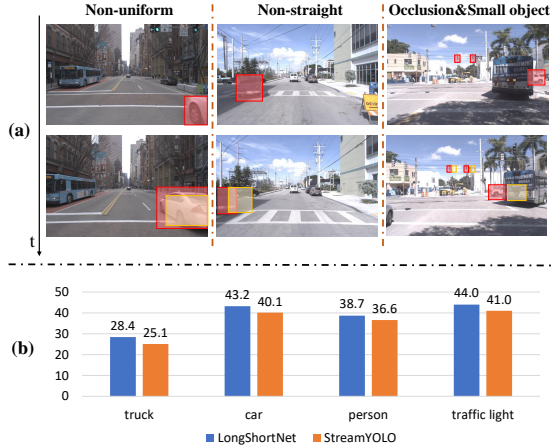


Fig. 2: Display of complex autonomous driving scenarios. (a) shows some suboptimal cases of StreamYOLO [16], where red and orange boxes denote ground truth and predictions, respectively. (b) shows the sAP comparison of LongShortNet and StreamYOLO. More examples are at <https://rebrand.ly/wgtclou>.

as non-uniform, non-straight, and occlusion). As shown in Fig. 2(a), StreamYOLO [16] 1) cannot accurately locate objects in real complex scenes, and 2) even misses occluded and tiny objects. The quantitative results in Fig. 2(b) further depict that *fusing temporal motion with spatial details can indeed improve perception accuracy*. Otherwise, it will endanger human life by making decision errors in autonomous driving. This problem even becomes more severe as vehicle speed and scene complexity increase.

However, *how to fuse spatiotemporal features without increasing latency is an open and challenging problem in streaming perception*. Although the previous VOD explored spatial-temporal aggregation [23, 4, 5, 6, 20, 24, 25] and spatial-temporal alignment [3, 21, 26] to mine more temporal motion with spatial semantic from support frames, they mostly explore offline settings and cannot handle online streaming perception. To address this issue, we propose a novel dual-path network named *LongShortNet* to calibrate long-term temporal with short-term spatial and model accurate motion coherence for streaming perception. To elaborate, we investigated the setup of various Long-Short Fusion Module (LSFM), and successfully brought spatiotemporal fusion strategies from traditional VOD to streaming perception. Supported by *spatiotemporal fusion* and *dilation-compression acceleration* strategies, LongShortNet achieves a satisfactory trade-off between effectiveness and efficiency. In summary, the contributions are summarized as three folds:

- To the best of our knowledge, LongShortNet is the *first end-to-end model* to learn long-term motion consistency for streaming perception, which endows the network with the ability to *handle more complex auto-driving scenarios*.
- We investigated Long-Short Fusion Module (LSFM) to calibrate the *long-term temporal* with *short-term spatial* with a simple but effective *dilation strategy*, ignoring the com-

plex solution of explicitly motion consistency supervised.

- LongShortNet achieves 37.1% (normal size (600, 960)) and 42.7% (large size (1200, 1920)) sAP *without using any extra data*, which outperforms the existing SOTA StreamYOLO [16] *with almost the same time cost* (20.2 ms vs. 20.1 ms). Moreover, LongShortNet works well on stricter metrics and small objects.

2. METHODOLOGY

2.1. LongShortNet

We argue that *spatial semantics* and *temporal motion* are critical for detecting complex movements such as non-uniform, non-linear, and occlusion. However, the existing methods [15, 16] have yet to explore temporal motion, let alone how to incorporate spatial semantics. Thus, we propose *LongShortNet* to coherently model long-term temporal and fuse it with short-term semantics. Particularly, LongShortNet consists of *ShortPath* and *LongPath*. As shown in Fig. 3(a), the frame sequence captured by the camera is divided into two parts, i.e., the current frame and the support frame. First, they are fed into ShortPath and LongPath, respectively, to generate spatial and temporal features. Next, a Long-Short Fusion Module (LSFM) aggregates short-term spatial and long-term temporal to capture motion consistency for representation learning. Finally, a detection *head* predicts upcoming results based on the features produced by the proposed LSFM.

Formally, ShortPath takes the current frame I_t as input and outputs spatial features $F_t = \mathcal{F}(I_t)$, where $\mathcal{F}(\cdot)$ is CNN networks, which includes the backbone (CSPDarknet-53 [27]) and the neck (PANet [28]). Similarly, LongPath stores temporal features $F_{t-i\delta t} = \mathcal{F}(I_{t-i\delta t})$, $i \in [1, N]$ where N and δt denote the number of frames and time steps, respectively. $\mathcal{F}(\cdot)$ represents the network of LongPath. Note that the backbone of Short/Long paths is weight-shared. By introducing tunable parameters N and δt , LongPath can capture more long-term temporal for fine movement reasoning. Then LSFM aggregates all features through $F_{fuse} = \text{LSFM}(F_t, \dots, F_{t-N\delta t})$, where F_{fuse} denotes the fused features generated by LSFM. The details of LSFM(\cdot) are described in the next section. Finally, the results are acquired by $D_{res} = \mathcal{H}(F_{fuse})$, where \mathcal{H} denotes the detection head (TALHead [16]) and D_{res} are predicted locations, scores, and categories.

2.2. Long Short Fusion Module

The previous streaming perception work [16] only *roughly concatenates the features of the last two frames*, without exploiting temporal motion and spatial semantics. To address this issue, we utilize Long-Short Fusion Module (LSFM) to efficiently aggregate short-term semantic/long-term temporal features $F_t/\{F_{t-i\delta t}, i \in [1, N]\}$ from Short/LongPath for more accurate motion perception. To our knowledge, we are *the*

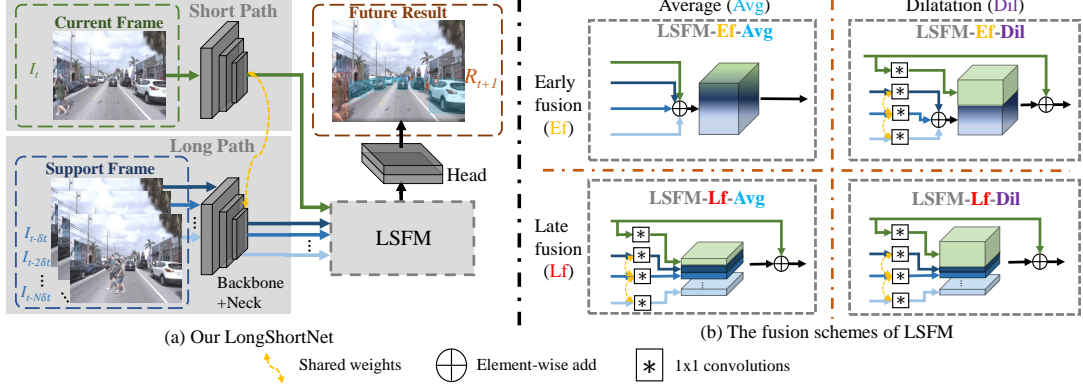


Fig. 3: Illustration of our LongShortNet. (a) is an overview of LongShortNet. (b) shows the details of different fusion schemes of LSFM.

first to explore how to fuse temporal motion and spatial semantics in streaming perception. We investigate a variety of feature aggregation ways, including 1) early fusion vs. late fusion and 2) average (equal weights) vs. dilatation (different weights). In summary, we verified four types of LSFM as shown in Fig. 3(b), denoted as LSFM-Ef-Avg, LSFM-Ef-Dil, LSFM-Lf-Avg, and LSFM-Lf-Dil.

Average-Early-Fusion. The LSFM-Ef-Avg process fuses the spatial semantics of each frame in LSFM and outputs pre-averaged synthetic spatiotemporal features for the detection head. This vanilla version allocates equal importance to the features of all frames, which is defined as,

$$F_{fuse} = \sum_{i=1}^N F_{t-i\delta t} + F_t, \quad (1)$$

where it counts all the features to fuse the current/historical spatial information directly and equally.

Dilatation-Early-Fusion. For LSFM-Ef-Dil, we investigate different weighting schemes for feature fusion as,

$$F_{fuse} = \text{Concat}(\mathcal{G}_{short}(F_t), \sum_{i=1}^N \mathcal{G}_{long}(F_{t-i\delta t})) + F_t, \quad (2)$$

where \mathcal{G} denotes the 1×1 convolution operation and Concat means the channel-wise concatenation. Supposed that the channel dimensionality of F_t and $F_{t-i\delta t}$ is d , all long-term temporal features are fused by addition before concatenating with the short-term spatial features. In this case, the output channels numbers of $\mathcal{G}_{short}(\cdot)$ and $\mathcal{G}_{long}(\cdot)$ are both $\lfloor d/2 \rfloor$. Note that we also adopt a residual connection to add current spatial features to enhance the historical temporal features.

Average-Late-Fusion. Contrary to the early fusion, LSFM-Lf-Avg fusion preserves the spatial semantic features of each frame separately and relies on the detection head to extract more high-level coherent features. It instantly concatenates all features without discriminating between ShortPath and LongPath, which is defined as,

$$F_{fuse} = \text{Concat}(\mathcal{G}_{avg}(F_t), \dots, \mathcal{G}_{avg}(F_{t-N\delta t})) + F_t, \quad (3)$$

where the output channels number of $\mathcal{G}_{avg}(\cdot)$ is $\lfloor d/(1+N) \rfloor$. LSFM-Lf-Avg treats all features equally, but our experiments have demonstrated that the current spatial features play a dominant role in streaming perception tasks.

Dilatation-Late-Fusion. We further propose LSFM-Lf-Dil, which enlarges the number of channels of ShortPath and forces LongShortNet to pay more attention to the current spatial information. Specifically, LSFM-Lf-Dil is defined as,

$$F_{fuse} = \text{Concat}(\mathcal{G}_{short}(F_t), \dots, \mathcal{G}_{long}(F_{t-N\delta t})) + F_t, \quad (4)$$

where two 1×1 convolution operations are employed to project F_t and $F_{t-i\delta t}$ separately. The output channels numbers of $\mathcal{G}_{short}(\cdot)$ and $\mathcal{G}_{long}(\cdot)$ are $\lfloor d/2 \rfloor$ and $\lfloor d/2N \rfloor$. After extensive experimental comparison, we finally chose Dilatation-Late-Fusion as LSFM and set N and δt to 3 and 1. Please refer to Sec. 3.4 for more details.

3. EXPERIMENTS

3.1. Dataset and Metric

Our experiments are carried out on the streaming perception dataset, i.e., Argoverse-HD [15]. Consistent with the previous works [15, 16], we employ the evaluation metric, streaming Average Precision (sAP). In addition, we also adopt the same train/val split as previous work [15, 16].

3.2. Implementation Details

LongShortNet is fine-tuned from the COCO [29] pre-trained model by 8 epochs, and the batch size is set to 16. We utilize YOLOX [30] with different model sizes (YOLOX-S, YOLOX-M, YOLOX-L) as our base detectors (corresponding to LongShortNet-S, LongShortNet-M, LongShortNet-L) and also employ the same loss function as [16]. Moreover, we slightly revamp the buffer scheme [16] to ensure the real-time performance of our network. For fair comparisons, all the other settings of hyperparameters follow the previous work [16]. Experiments are conducted on 4 NVIDIA V100 GPUs.

3.3. Comparison with SOTA Methods

The comparison with the state-of-the-art works on Argoverse-HD [15] is listed in Tab. 1. The upper and middle parts are the existing non-real-time and real-time streaming perception methods. From Tab. 1, we can see that the proposed LongShortNet outperforms all the real-time and non-real-time baselines with the performance of 37.1%. It is worth noting

Table 1: Comparison with non-real-time and real-time SOTA methods. ‘S=600/900’ means the short edge of the input image is 600/900. ‘†’ denotes adopting larger input size (1200, 1920). Results shown in blue font highlight the comparisons in stricter and harder metrics (sAP₇₅ and sAP_s).

Methods	sAP	sAP ₅₀	sAP ₇₅	sAP _s	sAP _m	sAP _l
Non-real-time detector-based methods						
Streamer (S=900) [15]	18.2	35.3	16.8	4.7	14.4	34.6
Streamer (S=600) [15]	20.4	35.6	20.8	3.6	18.0	47.2
Streamer + AdaS [17, 22]	13.8	23.4	14.2	0.2	9.0	39.9
Adaptive Streamer [22]	21.3	37.3	21.1	4.4	18.7	47.1
Real-time detector-based methods						
StreamYOLO-S [16]	28.8	50.3	27.6	9.7	30.7	53.1
StreamYOLO-M [16]	32.9	54.0	32.5	12.4	34.8	58.1
StreamYOLO-L [16]	36.1	57.6	35.6	13.8	37.1	63.3
LongShortNet-S	29.8	50.4	29.5	11.0	30.6	52.8
LongShortNet-M	34.1	54.8	34.6	13.3	35.3	58.1
LongShortNet-L	37.1	57.8	37.7	15.2	37.3	63.8
LongShortNet-L [†]	42.7	65.4	45.0	23.9	44.8	61.7

Table 2: Inference time (NVIDIA V100) and FLOPs (input size (600, 960)) for LongShortNet vs. StreamYOLO. Only the results for the large model are illustrated, which is the most time-consuming. The increased values are shown in blue font.

Methods	Inference time (ms/frame)	FLOPs (G)
StreamYOLO-L [16]	20.1	222.5
LongShortNet-L	20.2 (+0.1)	223.1 (+0.6)

that the sAP is further improved to 42.7% with larger input sizes without using any extra data. This fully demonstrates the effectiveness of LongShortNet.

Specifically, streamer [15] is a detector-based method that integrates the association and dynamic scheduling to overcome temporal aliasing, but achieves only 20.4% sAP due to the drawbacks of the non-real-time attribute. The recent approach [16] introduces an end-to-end model that produces results in the inference phase directly, achieving 36.1% sAP. However, the short-term temporal information offers unstable motion consistency, which damages the final performance. Meanwhile, the results listed in Tab. 2 also show that LongShortNet brings almost negligible increase of inference time cost (**20.2 ms vs. 20.1 ms**), even if it integrates triple times of historical features compared to StreamYOLO [16] (Refer to Sec. 3.4 for more details). It is also worth noting that LongShortNet obtains better performance in a stricter metric (sAP₇₅) and for small objects (sAP_s). This attractive observation again indicates that the long-term temporal features boost the performance in complex scenarios. We also notice that the sAP_l decreases when adopting the large input size and it is ascribed to the insufficient size of the receptive field. In other words, a better performance will be reached when this problem is tackled, and we leave this for future work.

3.4. Ablation Study

Effects of temporal range. To verify the effect of temporal range, we conduct ablation studies on N and δt , which are listed in Tab. 3. Note that (0, -) represents that only the current frame is adopted, and (1, 1) can be regarded as StreamYOLO [16]. As shown in Tab. 3, the best performance achieved by S/M/L LongShortNets achieves absolute improvements of 3.0, 4.4 and 4.5, and their (N , δt) values are (3, 1), (4, 2) and (3, 1). This manifests that the long-term temporal cues can reasonably model motion consistency. In addition, we notice

Table 3: The ablation study of N and δt . The best two results, the worst one and the improvements are shown in green, orange, red and blue fonts.

(N , δt)	LongShortNet-S	LongShortNet-M	LongShortNet-L
(0, -)	26.8	29.8	32.6
(1, 1)	28.7	33.5	36.1
(1, 2)	28.9	33.8	36.2
(2, 1)	29.2	34.0	36.7
(2, 2)	29.1	34.0	36.4
(3, 1)	29.8 \uparrow +3.0	34.1	37.1 \uparrow +4.5
(3, 2)	29.7	34.1	36.7
(4, 1)	29.2	34.0	37.0
(4, 2)	28.8	34.2 \uparrow +4.4	36.6
(5, 1)	29.3	33.4	36.9
(5, 2)	28.1	33.6	36.3

Table 4: The ablation study of LSFM. ‘**’ denotes removing residual connection. The improvements are shown in blue font.

LSFM	LongShortNet-S	LongShortNet-M	LongShortNet-L
LSFM-Ef-Avg	27.1	31.7	35.3
LSFM-Ef-Dil	28.6	33.2	36.1
LSFM-Lf-Avg	28.9	33.7	36.7
LSFM-Lf-Dil	29.8 (+2.7)	34.1 (+2.4)	37.1 (+1.8)
LSFM-Lf-Dil*	27.6	32.1	35.3

that the performance slightly drops if the temporal range is too large, especially for the smaller size model LongShortNet-S. Therefore, the relation between optimal temporal range and model sizes and how to choose a temporal range automatically are interesting topics for future work.

Effects of aggregation forms. To explore suitable long-term fusion strategies, we conduct ablation studies on LSFM. As shown in Tab. 4, the late fusion with dilation strategy obtains the best results in the S/M/L models, which indicates that the proposed LSFM-Lf-Dil module is able to aggregate short-term semantic and long-term temporal features in a more reasonable way. Note that StreamYOLO [16] has explored several fusion operations. It discovers that the concatenation operation, which is similar to our LSFM-Lf-Avg, stands out when considering both network parameters and inference speed. In addition, the performance drops when removing residual connection, which manifests that the current semantic features are crucial.

Efficiency analysis. As the number of input frames increases, the computational cost will simultaneously increase. Equipped with the buffer scheme [16], which stores the feature maps produced by the neck with a feature buffer, LongShortNet only employs three more 1×1 convolutional operations than StreamYOLO [16] to project the outputs of the neck to a suitable dimension. The inference time and FLOPs are shown in Tab. 2, which indicates that LongShortNet with long-range motion consistency capturing reduces almost all extra time costs compared to StreamYOLO [16].

4. CONCLUSION

This paper proposes an end-to-end dual-path network dubbed LongShortNet, which captures long-term temporal motion and calibrates it with short-term spatial semantics for real-time perception. Moreover, we investigate a Long-Short Fusion Module to explore spatiotemporal feature fusion. In the future, we will further investigate the integration of explicit motion consistency constraints based on geometry context.

5. REFERENCES

- [1] H. Ye, G. Wang, Y. Lu, and et al., “Multi-focus guided semantic aggregation for video object detection,” in *ICASSP*, 2022, pp. 4723–4727.
- [2] Z. Chen, W. Li, C. Fei, and et al., “Spatial-temporal feature aggregation network for video object detection,” in *ICASSP*, 2020, pp. 1858–1862.
- [3] W. Han, P. Khorrami, T. Paine, and et al., “Seq-nms for video object detection,” *CoRR*, vol. abs/1602.08465, 2016.
- [4] X. Zhu, Y. Xiong, J. Dai, and et al., “Deep feature flow for video recognition,” in *CVPR*, 2017, pp. 4141–4150.
- [5] X. Zhu, Y. Wang, J. Dai, and et al., “Flow-guided feature aggregation for video object detection,” in *ICCV*, 2017, pp. 408–417.
- [6] X. Zhu, J. Dai, L. Yuan, and et al., “Towards high performance video object detection,” in *CVPR*, 2018, pp. 7210–7218.
- [7] H. Wang, J. Tang, X. Liu, and et al., “Ptseformer: Progressive temporal-spatial enhanced transformer towards video object detection,” in *ECCV*, 2022.
- [8] G. Sun, Y. Hua, G. Hu, and et al., “Efficient one-stage video object detection by exploiting temporal consistency,” in *ECCV*, 2022.
- [9] Y. Chen, Y. Cao, H. Hu, and et al., “Memory enhanced global-local aggregation for video object detection,” in *CVPR*, 2020, pp. 10334–10343.
- [10] J. Deng, Y. Pan, T. Yao, and et al., “Relation distillation networks for video object detection,” in *ICCV*, 2019, pp. 7022–7031.
- [11] M. Han, Y. Wang, X. Chang, and et al., “Mining inter-video proposal relations for video object detection,” in *ECCV*, 2020, vol. 12366, pp. 431–446.
- [12] H. Wu, Y. Chen, N. Wang, and et al., “Sequence level semantics aggregation for video object detection,” in *ICCV*, 2019, pp. 9216–9224.
- [13] Y. Cui, L. Yan, Z. Cao, and et al., “Tf-blender: Temporal feature blender for video object detection,” in *ICCV*, 2021, pp. 8118–8127.
- [14] M. Shvets, W. Liu, and A. Berg, “Leveraging long-range temporal relationships between proposals for video object detection,” in *ICCV*, 2019, pp. 9755–9763.
- [15] M. Li and D. Ramanan, “Towards streaming perception,” in *ECCV*, 2020, vol. 12347, pp. 473–488.
- [16] J. Yang, S. Liu, Z. Li, and et al., “Real-time object detection for streaming perception,” in *CVPR*, 2022, pp. 5385–5395.
- [17] T. Chin, R. Ding, and D. Marculescu, “Adascale: Towards real-time video object detection using adaptive scaling,” in *MLSys*, 2019.
- [18] F. He, N. Gao, J. Jia, and et al., “Queryprop: Object query propagation for high-performance video object detection,” in *AAAI*, 2022, pp. 834–842.
- [19] L. He, Q. Zhou, X. Li, and et al., “End-to-end video object detection with spatial-temporal transformers,” in *ACM MM*, 2021, pp. 1507–1516.
- [20] G. Sun, Y. Hua, G. Hu, and et al., “MAMBA: multi-level aggregation via memory bank for video object detection,” in *AAAI*, 2021, pp. 2620–2627.
- [21] P. Tang, C. Wang, X. Wang, and et al., “Object detection in videos by high quality object linking,” *TPAMI*, vol. 42, no. 5, pp. 1272–1278, 2020.
- [22] A. Ghosh, A. Nambi, A. Singh, and et al., “Adaptive streaming perception using deep reinforcement learning,” *CoRR*, vol. abs/2106.05665, 2021.
- [23] S. Wang, Y. Zhou, J. Yan, and et al., “Fully motion-aware network for video object detection,” in *ECCV*, 2018, vol. 11217, pp. 557–573.
- [24] F. Xiao and Y. Lee, “Video object detection with an aligned spatial-temporal memory,” in *ECCV*, 2018, vol. 11212, pp. 494–510.
- [25] G. Bertasius, L. Torresani, and J. Shi, “Object detection in video with spatiotemporal sampling networks,” in *ECCV*, 2018, vol. 11216, pp. 342–357.
- [26] H. Belhassen, H. Zhang, V. Fresse, and et al., “Improving video object detection by seq-bbox matching,” in *VISAPP*, 2019, pp. 226–233.
- [27] A. Bochkovskiy, C. Wang, and H. Liao, “Yolov4: Optimal speed and accuracy of object detection,” *CoRR*, vol. abs/2004.10934, 2020.
- [28] S. Liu, L. Qi, H. Qin, and et al., “Path aggregation network for instance segmentation,” in *CVPR*, 2018, pp. 8759–8768.
- [29] T. Lin, M. Maire, S. Belongie, and et al., “Microsoft COCO: common objects in context,” in *ECCV*, 2014, vol. 8693, pp. 740–755.
- [30] Z. Ge, S. Liu, F. Wang, and et al., “YOLOX: exceeding YOLO series in 2021,” *CoRR*, vol. abs/2107.08430, 2021.